S-Phase Duration Is the Main Target of Cell Cycle Regulation in Neural Progenitors of Developing Ferret Neocortex

Miguel Turrero García, YoonJeung Chang, Yoko Arai, and Wieland B. Huttner*

Max Planck Institute of Molecular Cell Biology and Genetics, 01307 Dresden, Germany

ABSTRACT

The evolutionary expansion of the neocortex primarily reflects increases in abundance and proliferative capacity of cortical progenitors and in the length of the neurogenic period during development. Cell cycle parameters of neocortical progenitors are an important determinant of cortical development. The ferret (*Mustela putorius furo*), a gyrencephalic mammal, has gained increasing importance as a model for studying corticogenesis. Here, we have studied the abundance, proliferation, and cell cycle parameters of different neural progenitor types, defined by their differential expression of the transcription factors Pax6 and Tbr2, in the various germinal zones of developing ferret neocortex. We focused our analyses on postnatal day 1, a late stage of cortical neurogenesis when upper-layer neurons are produced. Based on cumulative 5-ethynyl-2'-deoxyuridine (EdU) labeling as well as Ki67 and proliferating cell nuclear antigen (PCNA) immunofluorescence, we determined the duration of the various cell cycle phases of the different neocortical progenitor subpopulations. Ferret neocortical progenitors were found to exhibit longer cell cycles than those of rodents and little variation in the duration of G1 among distinct progenitor types, also in contrast to rodents. Remarkably, the main difference in cell cycle parameters among the various progenitor types was the duration of S-phase, which became shorter as progenitors progressively changed transcription factor expression from patterns characteristic of self-renewal to those of neuron production. Hence, S-phase duration emerges as major target of cell cycle regulation in cortical progenitors of this gyrencephalic mammal. J. Comp. Neurol. 524:456–470, 2016.

During mammalian evolution, certain species have experienced an expansion of their neocortical surface, mainly due to the presence of an increased number of neurons and glial cells. The neocortex of these species is folded into grooves (sulci) and ridges (gyri), a trait known as gyrencephaly, as opposed to lissencephaly, in which the cortical surface is smooth (Lewitus et al., 2013; Zilles et al., 2013). To understand cortical expansion, it is necessary to study the developmental mechanisms underlying it, especially the roles played by the various types of neural progenitors with varying degrees of self-renewing and neurogenic capacities and the processes that regulate their neuron output (Fietz and Huttner, 2011; Florio and Huttner, 2014; Franco and Muller, 2013; Kriegstein et al., 2006; Lewitus et al., 2013; Lui et al., 2011; Zilles et al., 2013).

One important factor is the duration of their cell cycle and each of its constituent phases, which are considered key determinants of the proliferation versus

Dr. Turrero García's Department of Neurobiology, Harvard Medical School, 220 Longwood Avenue, Boston, MA 02115

Dr. Chang's Program in Molecular Medicine, University of Massachusetts Medical School, Worcester, MA 01605-2377

Dr. Arai's Institut Jacques-Monod/Université Paris Diderot, Bâtiment Buffon 516B, 15 rue Hélène Brion 75205, Paris Cedex 13, France

*CORRESPONDENCE TO: Wieland B. Huttner, Max Planck Institute of Molecular Cell Biology and Genetics, Pfotenhauerstrasse 108, 01307 Dresden, Germany. E-mail: huttner@mpi-cbg.de

differentiation balance in cortical progenitors (Borrell and Calegari, 2014; Caviness and Takahashi, 1995; Dehay and Kennedy, 2007; Götz and Huttner, 2005; Takahashi et al., 1995). Here, we aim to compare the cell cycle features of different neural progenitor types in the developing neocortex of the ferret (*Mustela putorius furo*), a gyrencephalic carnivore, in an effort to understand the developmental basis of its evolutionary expansion.

The dorsolateral telencephalon is the site of origin of the majority of neocortical neurons, which are born from neural progenitors located in its proliferative areas, migrating away from them to form the mature cortex. The first proliferative area, the ventricular zone (VZ), is populated by apical progenitors (APs), a collective term for neuroepithelial (NE) cells and the highly related radial glia (RG), into which NE cells transform at the onset of neurogenesis. APs characteristically express the transcription factor Pax6. They exhibit apicobasal polarity, with cellular processes contacting both the apical (ventricular) and the basal (pial) surfaces of the cortical wall. APs divide at the ventricular surface, initially in a symmetric self-renewing manner that expands the progenitor pool, later switching to an asymmetric self-renewing mode that maintains the pool while generating neurons and other progenitor types (Götz and Huttner, 2005; Kriegstein and Alvarez-Buylla, 2009; Taverna et al., 2014).

After the onset of neurogenesis, a new proliferative area appears basally from the VZ: the subventricular zone (SVZ). In many mammalian species, this area is progressively subdivided into two subregions, the inner subventricular zone (ISVZ) and the outer subventricular zone (OSVZ), which appears later in development and is greatly expanded in gyrencephalic species (Cheung et al., 2007; Fish et al., 2008; Franco and Muller, 2013; Kriegstein et al., 2006; Lui et al., 2011; Martinez-Cerdeno et al., 2012; Smart et al., 2002). The SVZ harbors a variety of neural progenitors, collectively referred to as basal progenitors, which eventually become the main source of neocortical neurons.

Basal intermediate progenitors (bIPs) are multipolar cells with no known polarity cues; they express the transcription factor Tbr2, and in mouse typically undergo a terminal symmetric division, generating two neurons (Englund et al., 2005; Haubensak et al., 2004; Miyata et al., 2004; Noctor et al., 2004). A subpopulation of bIPs with self-renewing capacity has been reported in the rodent (Noctor et al., 2004) and human neocortex (Hansen et al., 2010; LaMonica et al., 2013). Their abundance has been speculated to be at least partially responsible for the expansion of the neocortex in gyrencephalic species (Lui et al., 2011).

Basal radial glia (bRG) are a recently described progenitor type, defined as Pax6-positive, Tbr2-negative

monopolar progenitors that keep a basal process throughout their cell cycle (Fietz et al., 2010; Hansen et al., 2010; Reillo et al., 2011). They normally undergo self-renewing divisions, either symmetric or asymmetric, generating neurons (as is the case in the mouse: Shitamukai et al., 2011; Wang et al., 2011) or other progenitor types (as in human and ferret: Gertz et al., 2014; Hansen et al., 2010; LaMonica et al., 2013). A recent report has described great morphologic variability in primate bRG: they can present or grow either a single process or two, directed apically and/or basally and not necessarily contacting the apical or basal surfaces of the cortical wall (Betizeau et al., 2013). bRG are present in both lissencephalic and gyrencephalic species, normally in a much higher proportion in the latter (Fietz et al., 2010; Hansen et al., 2010; Kelava et al., 2012; Reillo et al., 2011; Shitamukai et al., 2011; Wang et al., 2011). They have been proposed to play a significant role in the development of gyrencephaly, both as a source of neurons and as a scaffolding element (Borrell and Reillo, 2012; Fietz and Huttner, 2011; Lui et al., 2011); however, their abundance alone does not account for the presence or absence of cortical folding (Kelava et al., 2012).

Studies in mouse have shown that cell cycle duration increases throughout the proliferative areas along neurogenesis, correlating with the loss of the self-renewing capacity of neural progenitors and the concomitant increase in their neurogenic output (Calegari et al., 2005; Caviness and Takahashi, 1995; Takahashi et al., 1995). This cell cycle lengthening reflects an increase in bIP abundance, as it is mainly due to the lengthening of G1-phase in the transition from APs to bIPs (Arai et al., 2011; Calegari et al., 2005). The importance of the G1-phase in the switch from proliferation to differentiation was supported by experimental manipulations in which artificial lengthening of this phase was shown to cause premature neurogenesis (Calegari and Huttner, 2003), whereas its shortening had the opposite effect, leading to an expansion of the progenitor pool (Lange et al., 2009; Pilaz et al., 2009).

Interestingly, a recent report showed that mouse APs and bIPs committed to neurogenic division exhibit a shortening of S-phase, compared with those that maintain their self-renewal capacity (Arai et al., 2011). Observations of cell cycle shortening toward the end of neurogenesis in other species (Kornack and Rakic, 1998; Reillo and Borrell, 2012), as well as studies in the macaque showing that progenitors cycle faster when generating neurons for the supragranular-dense cortical area 17, compared with those in area 18 (Lukaszewicz et al., 2005), suggest a role of cell cycle length in both the regulation of greater neuron output

in specific areas during development and the overall generation of neurons in evolution.

In the present study, we studied the cell cycle of neural progenitors in the developing ferret neocortex. Building on previous studies (Fietz et al., 2010; Poluch and Juliano, 2015; Reillo and Borrell, 2012), we calculated the proportions of different progenitor types, as distinguished by their expression of Pax6 and/or Tbr2, throughout the entire neurogenic period. To calculate the duration of each cell cycle phase of cortical progenitors, we performed in vivo cumulative S-phase labeling with 5-ethynyl-2′-deoxyuridine (EdU) on newborn ferret kits, during late neurogenesis. We analyzed the rate of incorporation of this thymidine analogue into cycling cells, considering each progenitor type separately. We found that, in contrast to what has been described in the mouse, there was little variation in the duration of G1-phase between progenitors. The S-phase shortening as progenitors restrict their fate and self-renewing capacity was much more relevant, accounting for most of the variation in cell cycle length that we observed.

MATERIALS AND METHODS

All experiments involving animal use were performed in accordance with German animal welfare legislation, and were approved by the Landesdirektion Sachsen. The housing and caretaking of the ferrets always followed the recommendations of the breeder. All experiments and handling protocols were carefully and thoroughly designed and carried out so as to minimize any potential suffering or stress caused to the animals.

Animals

Timed-pregnant sable ferrets (*Mustela putorius furo*) were purchased from Marshall BioResources (North Rose, NY, USA). They were delivered to Dresden at gestation days 20–28, with the breeding day defined as day 0. Pregnant jills were housed at the facilities of Bio-Crea (GmbH, Radebeul, Saxony, Germany).

Cumulative EdU labeling

Ferret kits were injected intraperitoneally with 100 µg of EdU diluted in phosphate-buffered saline (PBS; 100 µl from a 1-mg/ml stock). The injections were performed every 3 hours, and the kits were sacrificed at the corresponding times, for a period of up to 48 hours. So as to minimize the stress of all the animals, the ferret kits remained with their mother and their littermates throughout the whole experiment, except for the brief injection and sacrifice times, during which they were transferred onto a heating blanket. The duration of each cell cycle phase was calculated based on the model of linear S-phase incorporation, as previously described (Nowakowski et al., 1989).

Determination of T_C and T_S

We performed double immunofluorescence staining for Pax6 and Tbr2, accompanied by chemical detection of EdU, and quantified the proportion of EdU-labeled cells within each progenitor population in the VZ, ISVZ, and OSVZ at 13 different time points (Fig. 3). By plotting the rate of incorporation of EdU for each progenitor population versus the time of cumulative labeling, and taking into account the proportion of cycling cells we had calculated previously (Fig. 3C, arrows), which was corroborated by the plateaus in our plotted graphs (Fig. 3C, dashed horizontal lines), we were able to directly obtain the duration of their cell cycle minus S-phase (T_C-T_S), thereafter calculating the duration of S-phase (T_S) and the total cell cycle length (T_C) (Fig. 3C, Table 1) (Nowakowski et al., 1989).

Determination of T_{G2}

The progenitors that take up EdU during S-phase continue cycling through G2-phase and enter mitosis; the half-time of full mitotic labeling can thus be used as an average for T_{G2} in any given population (Arai et al., 2011). We used phosphorylated histone H3 (PH3) as a mitotic marker, and performed double-immunofluorescence staining for PH3 and either Pax6 or Tbr2, combined with chemical detection of EdU (Fig. 4A–D). Because of the limited number of detection channels when immunofluorescence experiments were performed, our estimates only considered either Pax6 or Tbr2 alongside PH3 and EdU. Because almost all of the Tbr2+ mitoses were Pax6+ in all areas (VZ: 100%; ISVZ: 92.8 ± 11.0%; OSVZ: 88.9 ± 21.4% [mean ± SD, n = 9 kits from 9 litters]), whereas not all Pax6+ mitoses were Tbr2+ (VZ: 14.0 ± 12.1%; ISVZ: 69.0 ± 9.1%; OSVZ: 46.3 ± 17.4% [mean ± SD, n = 9 kits from 9 litters]), we arbitrarily ascribed the T_{G2} values calculated for Tbr2+ cells to both Pax6+ & Tbr2+ and Pax6− & Tbr2+ progenitors, and those calculated for Pax6+ cells to Pax6+ & Tbr2− progenitors. If these populations could be separately analyzed, the T_{G2} values might differ slightly from our estimates; however, because the differences in T_{G2} between populations are minimal (Fig. 4E, Table 1), this would have no major effect on the overall results and conclusions presented here.

Determination of T_M

We calculated the duration of mitosis (T_M) by extrapolating the proportion of mitotic cells within each actively cycling population to the total duration of their cell

TABLE 1.
Cell Cycle Parameters of P1 Ferret Neocortical Progenitors[1]

Area	Progenitor type	Method	T_C-T_S	T_S (% of T_C)	T_C	T_{G2}	T_M	T_{G1} (% of T_C)
VZ	Pax6+ Tbr2−	**Ki67**	**33.7**	**16.1 (32.3)**	**49.8**	**2.0**	**1.2**	**30.5 (61.2)**
		EdU	39.4	16.1 (28.9)	55.5	2.0	1.3	36.1 (65.0)
	Pax6+ Tbr2+	**Ki67**	**36.4**	**19.7 (35.1)**	**56.1**	**2.0**	**0.5**	**33.9 (60.4)**
		EdU	38.8	19.7 (33.7)	58.5	2.0	0.5	36.3 (62.1)
ISVZ	Pax6+ Tbr2−	**Ki67**	**35.5**	**8.6 (19.6)**	**44.1**	**2.2**	**0.8**	**32.5 (73.7)**
		EdU	40.8	8.6 (17.5)	49.4	2.2	0.9	37.7 (76.3)
	Pax6+ Tbr2+	**Ki67**	**34.3**	**9.4 (24.8)**	**43.7**	**2.0**	**0.8**	**31.5 (72.8)**
		EdU	32.6	9.4 (22.4)	42.0	2.0	0.7	28.6 (68.1)
	Pax6− Tbr2+	**Ki67**	**36.0**	**1.9 (4.4)**	**37.9**	**1.7**	**2.0**	**32.3 (85.2)**
		EdU	43.9	1.9 (4.2)	45.8	1.7	2.4	39.8 (86.9)
OSVZ	Pax6+ Tbr2−	**Ki67**	**46.1**	**22.6 (32.9)**	**68.7**	**2.1**	**1.5**	**42.5 (61.9)**
		EdU	48.7	22.6 (31.7)	71.3	2.1	1.6	45.0 (63.1)
	Pax6+ Tbr2+	**Ki67**	**34.4**	**9.7 (22.0)**	**44.1**	**1.9**	**0.9**	**31.5 (71.4)**
		EdU	35.3	9.7 (21.6)	45.0	1.9	1.0	32.4 (72.0)
	Pax6− Tbr2+	**Ki67**	**35.6**	**3.1 (7.9)**	**38.7**	**1.7**	**0.9**	**33.0 (85.3)**
		EdU	38.2	3.1 (7.5)	41.3	1.7	0.9	35.6 (86.2)

[1]Horizontal rows indicated by "Ki67" provide cell cycle phase values obtained by determining the proportion of cycling progenitors from the Ki67 data shown in Figure 2C; these cell cycle phase values are summarized in Figure 5. Horizontal rows indicated by "EdU" provide cell cycle phase values obtained by determining the proportion of cycling progenitors from the plateau of cumulative EdU labeling shown in Figure 3C, dashed lines. The T_{G2} values are from Figure 4E and F and were applied as follows: the Pax6 values (Fig. 4E) for Pax6+ & Tbr2− progenitors; the Tbr2 value (Fig. 4F) for Pax6− & Tbr2+ progenitors; the mean of Pax6 and Tbr2 values for Pax6+ Tbr2+ progenitors.

Abbreviations: VZ, ventricular zone; ISVZ, inner subventricular zone; OSVZ, outer subventricular zone; T_C, duration of cell cycle; T_S, duration of S-phase; T_{G2}, duration of G2-phase; T_{G1}, duration of G1-phase; T_M, duration of mitosis.

cycle. For this purpose, we used data from 19 ferret samples from the first 24 hours of the cumulative labeling experiment, because the progenitor type and cycling cell proportions did not change significantly after 24 hours of cumulative EdU labeling (data not shown). We counted the average number of cells undergoing mitosis, based on PH3 and 4′-6-diamidino-2-phenylindole (DAPI) staining (VZ: 5.6 ± 2.2; ISVZ: 9.6 ± 3.8; OSVZ: 5.8 ± 2.8 [mean ± SD mitotic cells per 250 μm of ventricular surface, $n = 19$]), as well as the number of cycling cells in each area (VZ: 294.2 ± 56.3; ISVZ: 538.1 ± 116.1; OSVZ: 287.1 ± 113.6 [mean ± SD number of Ki67+ cells per 250 μm of ventricular surface, $n = 19$]). The proportion of each progenitor population within the cycling cells in each area (Fig. 2C), and the proportion of mitotic cells belonging to each population (Fig. 4F), were calculated from untreated animals ($n = 9$ kits from 9 litters). By combining these results, we obtained an estimation of the proportion of mitotic cells within the cycling fraction of each progenitor population. We obtained estimates for T_M by extrapolating these proportions to the T_C of each population (Table 1).

Tissue collection and fixation

For the analysis of ferret embryos, pregnant jills were deeply anesthetized by intramuscular injection of ketamine (20 mg/kg) plus xylazine (1 mg/kg); the embryos were collected in PBS, and the jill was then sacrificed by intracardiac injection of T-61 (0.3 ml/kg). The whole heads of the embryos (at embryonic days [E] 20 and 24) or dissected brains (E28, E32, and E36) were briefly rinsed in PBS and immersed in 4% (w/v) paraformaldehyde (PFA) in phosphate buffer (120 mM in water, pH 7.2), in which they were fixed overnight (16–24 hours) at 4°C. For postnatal stages, ferret kits were subjected to hypothermic anesthesia in crushed ice, and sacrificed by intracardiac perfusion with 4% PFA at 37°C. Their brains were dissected out, immersed in 4% PFA, and postfixed overnight at 4°C. After fixation, the tissue was briefly washed in PBS, and either stored at 4°C in PBS–azide (0.02% w/v sodium azide in PBS) or further processed for cryosectioning.

Immunofluorescence

For cryosectioning, fixed samples were cryoprotected by two successive overnight immersion steps in 15% and 30% (w/v) sucrose in PBS, carried out at 4°C. The samples were then embedded in OCT compound (Tissue-Tek, Sakura Finetek, Torrance, CA), and stored at −20°C. Then 10–20-μm-thick sections were obtained with a cryostat, and stored at −20°C until use. For immunofluorescence staining, cryosections were washed in PBS; heat-induced antigen retrieval was then performed at 70°C for 1 hour, in a sodium citrate solution (0.01 M in water, pH 6.0) containing glycerol (10% v/v). The slides were allowed to cool down to room temperature for 10–15 minutes, and then washed with

TABLE 2.
Primary Antibodies Used in This Study

Antigen	Description of Immunogen	Source, cat. #, RRID, host species	Dilution
Anti-Pax6	Peptide (QVPGSEPDMSQYWPRLQ) derived from the C-terminus of the mouse Pax-6 protein	Covance PRB-278P, RRID: AB_2313780, rabbit polyclonal	1:200
Anti-Tbr2	Synthetic peptide conjugated to KLH derived from within residues 650 to the C-terminus of mouse TBR2/Eomes	Abcam ab23345, RRID: AB_778267, rabbit polyclonal	1:200
Anti-Tbr2	KLH-conjugated linear peptide corresponding to mouse Tbr2	Millipore AB15894, RRID: AB_10615604, chicken polyclonal	1:500
Anti-Tbr2	*E. coli*-derived recombinant human EOMES, Gly471–Pro686	R&D AF6166, RRID: AB_10569705, sheep polyclonal	1:200
Anti-Ki67	Human recombinant peptide corresponding to a 1002-bp Ki-67 cDNA fragment	Dako M7240, clone MIB-1, RRID: AB_2142367, mouse monoclonal	1:200
Anti-PCNA	Rat PCNA made in the protein A vector pR1T2T	Millipore MAB424, clone PC10, RRID: AB_95106, mouse monoclonal	1:200
Anti-PH3	Synthetic peptide conjugated to KLH, corresponding to amino acids 23–35 of human histone H3	Abcam ab10543, RRID: AB_2295065, rat monoclonal	1:500

PBS, permeabilized with 0.3% (v/v) Triton X-100 in PBS for 30 minutes, and quenched with 0.1 M glycine–Tris (pH 7.4) for 30 minutes. The sections were then washed with Tx buffer (300 mM NaCl, 0.2% v/v gelatin, 0.3% v/v Triton X-100 in PBS). Primary antibodies were diluted in the same buffer, and the sections were incubated with them overnight at 4°C. The sections were then washed with Tx, and incubated with secondary antibodies and DAPI, diluted in the same buffer, for 1–2 hours at room temperature. The slides were mounted with a coverslip, using either Mowiol or ProLong Gold Antifade Reagent (Molecular Probes, Eugene, OR), and stored at 4°C in the dark. Primary antibodies and dilutions are listed in Table 2. Donkey (1:500) or goat (1:1,000) secondary antibodies coupled to Alexa 488, Alexa 555, or Alexa 647 were used. For EdU detection, the Click-iT EdU Alexa Fluor 647 Imaging Kit (Invitrogen, Carlsbad, CA) was used, according to the supplier's instructions with slight modifications (Arai et al., 2011).

Antibody characterization

See Table 2 for a list of all antibodies used.

The specificity of the Pax6 antibody was characterized by western blot on mouse brain, recognizing two closely migrating bands around 50 kDa (Davis and Reed, 1996). The pattern of Tbr2 staining we observed in our experiments was consistently similar to that described in previous ferret studies (Fietz et al., 2010; Poluch and Juliano, 2015; Reillo et al., 2011), irrespective of manufacturer and host species. The rabbit Tbr2 antibody was characterized by western blot, detecting a 72-kDa band in cell lysates of EL4 cells expressing V5-tagged eomesodermin, and two bands of 85 and 75 kDa of either human mesendoderm or E14 mouse embryonic brains (manufacturer's information). The

specificity of the chicken Tbr2 antibody was tested by western blot on E13–14 mouse brain lysate. The sheep Tbr2 antibody was characterized by western blot on lysates of BG01V, mesendoderm-differentiated human embryonic stem cells, where it recognized specific bands at 85–105 kDa. The Ki67 antibody was characterized by western blot of IM-9 (multiple myeloma cell line) cell lysates, where it detected bands of 345 and 395 kDa, identical to the original Ki-67 antibody (manufacturer's information; Key et al., 1993). Additionally, the pattern of Ki67 staining we observed was similar to that of previous ferret studies using a different antibody (Reillo and Borrell, 2012). The proliferating cell nuclear antigen (PCNA) antibody detected a 36-kDa band (manufacturer's information), and displayed a uniform/punctate pattern of staining in ferret cortical progenitors similar to that described previously in the mouse (Arai et al., 2011). The specificity of the PH3 antibody was confirmed by western blot of HeLa nuclear lysates (manufacturer's information); its pattern of staining was identical to that observed with other antibodies against the same epitope in the ferret (Fietz et al., 2010; Poluch and Juliano, 2015; Reillo et al., 2011), and further confirmed in the developing telencephalon of other species (Kelava et al., 2012).

Image acquisition and analysis

Fixed tissue images were acquired either on a Zeiss LSM 510 or a Zeiss LSM 710 point scanning confocal microscope. Images used for cell counting were acquired as tile scans covering the dorsolateral telencephalon, and obtained from medial/frontomedial positions along the rostrocaudal axis of the brain. The images were acquired with a Zeiss C-Apochromat 40× 1.2 NA objective, as 1-μm-thick optical sections, at a

resolution of 2,048 × 2,048 pixels. Laser power, gain, and offset were adjusted for each sample and imaging session, maximizing the use of the dynamic range by avoiding under- or overexposure. Other objectives (Zeiss Plan- Apochromat 10×, 0.45 NA; Zeiss Plan-Apochromat 20×, 0.8 NA) and imaging conditions were used when necessary. The tile scan images were stitched with Zen software (Zeiss). All image analysis was performed with ImageJ, either in its standard version (http://rsbweb.nih.gov/ij/; RRID: nif-0000-30467) or in the Fiji distribution (http://fiji.sc/Fiji; RRID: SciRes_000137). Cell counting was performed with the Cell Counter ImageJ plug-in. After repositioning the image as necessary for the apical surface to be horizontal, 250-µm-wide windows were cropped from the different proliferative areas within the cortical wall. These areas (ventricular zone, inner subventricular zone, and outer subventricular zone) were identified based on their histological features as observed from DAPI staining. The regions selected for counting were located at least 200 µm away from the pallial/subpallial boundary. Any areas not readily identifiable, as well as any unclear borders between proliferative areas, were never included within counting windows. The contrast and brightness of the original images were adjusted as necessary for counting purposes, but never modified in the original files.

RESULTS

Cell subpopulations in the germinal zones during neurogenesis in the developing ferret neocortex

We first quantified the neural progenitor subpopulations present in the developing ferret neocortex, focusing on a medial position along the rostrocaudal axis of the telencephalon, in the prospective somatosensory cortex (Fig. 1A). Given that cortical neurons in this area are born approximately from E24 until postnatal day (P) 4 (Noctor et al., 1997), we analyzed six developmental stages (E20, E24, E28, E32, E36, and P1), thus covering most of the neurogenic period. We analyzed the germinal zones (Fig. 1B,C) for the presence of two transcription factors, Pax6 and Tbr2, known in mouse to be expressed in a sequential manner by cortical progenitors as they become progressively restricted to a neurogenic fate (Englund et al., 2005).

Quantification of Pax6 and Tbr2 immunoreactivity (Fig. 1D–I) revealed that the proportion of Pax6+ & Tbr2− cells in the germinal zones overall decreased with the progression of corticogenesis (Fig. 1J). This decrease reflected mostly the behavior of progenitors

in the VZ (Fig. 1K) rather than in the SVZ (Fig. 1L). In contrast, we observed an increase, in the course of corticogenesis, in the proportion of Pax6+ & Tbr2+ cells in the germinal zones overall (Fig. 1J), which again reflected mostly the behavior of progenitors in the VZ (Fig. 1K). The proportion of Pax6− & Tbr2+ cells decreased over time (Fig. 1J), in particular in the SVZ (Fig. 1L). In contrast, the proportion of Pax6− & Tbr2− cells, which were found to be mostly newborn neurons as revealed by beta-III tubulin staining (data not shown), increased with the progression of corticogenesis (Fig. 1J), notably in the SVZ (Fig. 1L), in line with the neuron output increasing at later stages of cortical neurogenesis. Accordingly, at P1, Pax6− & Tbr2− cells constituted the largest relative subpopulation in the OSVZ and Pax6+ & Tbr2+ cells the largest relative subpopulation in the ISVZ (Fig. 1M). Our results are consistent with previously published findings that analyzed the same transcription factors in mitotic cells in the developing ferret neocortex (Martinez-Cerdeno et al., 2012; Poluch and Juliano, 2015).

Cycling cell subpopulations in the germinal zones of P1 ferret neocortex

Next, we determined the cycling cells in each subpopulation in the germinal zones of newborn ferret kits at P1, a late neurogenic stage (Noctor et al., 1997). For this purpose, we performed triple immunofluorescence for Pax6, Tbr2, and the cycling cell marker Ki67 (Fig. 2A,B). When expressed as proportion of cycling cell subpopulation per germinal zone (Fig. 2D), and consistent with the data shown in Figure 1, Pax6+ & Tbr2− progenitors constituted the largest subpopulation of cycling cells in the VZ, followed by Pax6+ & Tbr2+ progenitors (Fig. 2D). Conversely, in the ISVZ, Pax6+ & Tbr2+ progenitors constituted the largest cycling cell subpopulation, followed by Pax6+ & Tbr2− progenitors. In the OSVZ, cycling Pax6+ & Tbr2− and Pax6+ & Tbr2+ progenitors were approximately equally abundant and together constituted the vast majority of cycling cells, as was the case for the VZ and ISVZ (Fig. 2D). In all three germinal zones, cycling Pax6− & Tbr2+ progenitors were very scarce, and cycling Pax6− & Tbr2− cells constituted only a minor subpopulation, increasing in proportion from the VZ to the OSVZ (Fig. 2D).

When the proportion of cycling cells was determined for each subpopulation and germinal zone (Fig. 2C), we found that not all of the Pax6+ & Tbr2− cells, Pax6+ & Tbr2+ cells, and Pax6− & Tbr2+ cells were cycling. Thus, only about 60–70% of the Pax6+ & Tbr2− population in each germinal zone was Ki67+ (Fig. 2C). Most
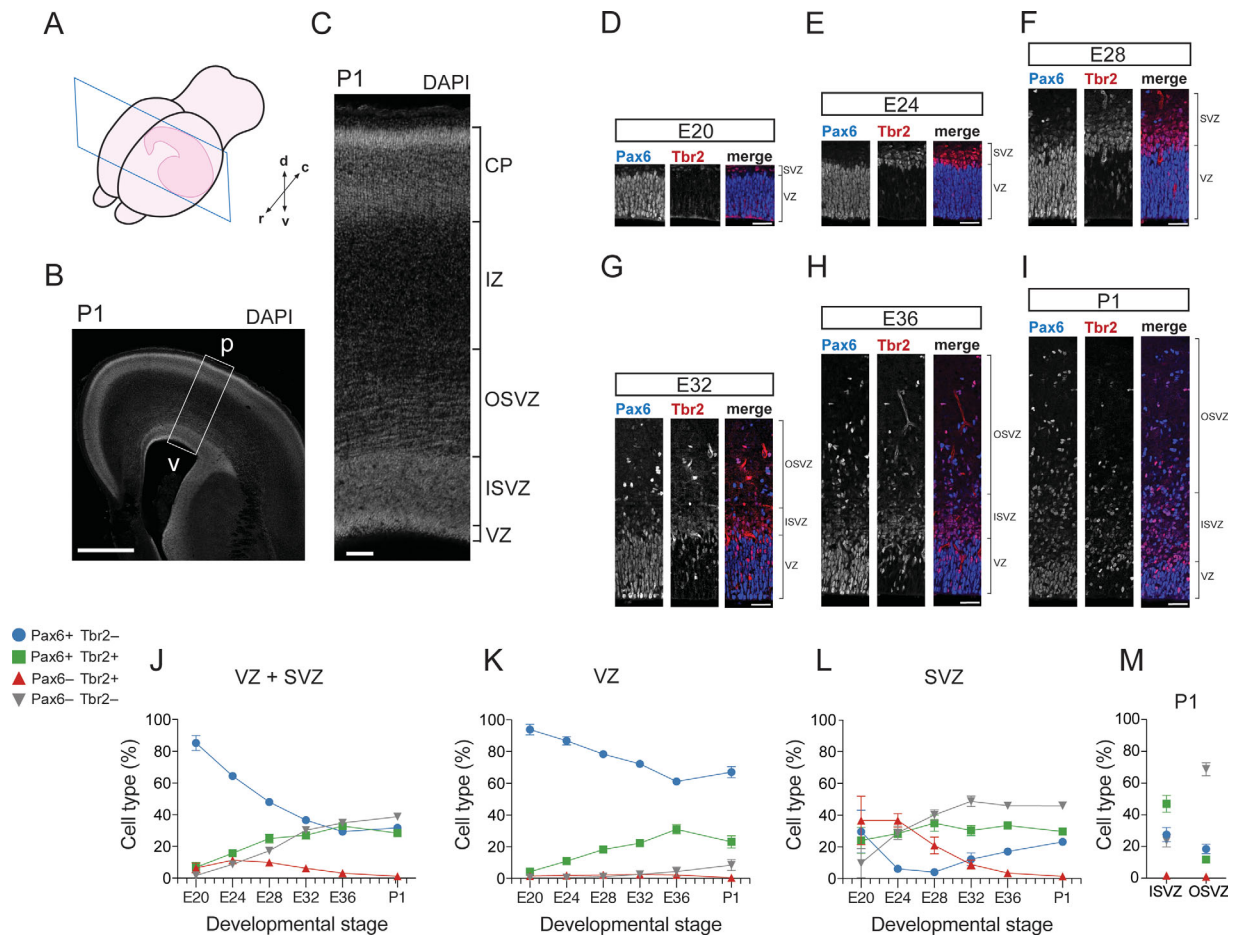
Figure 1. Pax6- and/or Tbr2-expressing cell subpopulations in the germinal zones of developing ferret neocortex. **A:** Cartoon showing a coronal section of a P1 ferret hemisphere, with the rostrocaudal (r–c) and dorsoventral (d–v) axes as indicated. **B,C:** DAPI staining of P1 ferret neocortex (100-μm coronal vibratome section, stack of four 2.5-μm optical sections). The box in B indicates the area shown at higher magnification in C. p, pial surface; v, ventricle. **D–I:** Double immunofluorescence for Pax6 (blue in merged images) and Tbr2 (red in merged images) on 20-μm coronal cryosections of ferret neocortex at the indicated stages (single 1-μm optical sections). **J–M:** Quantification of Pax6+ & Tbr2− (blue), Pax6+ & Tbr2+ (green), Pax6− & Tbr2+ (red) and Pax6− & Tbr2− (gray) nuclei in the VZ+SVZ (**J**), VZ (**K**), SVZ (**L**), and ISVZ vs. OSVZ (**M**) of ferret neocortex at the indicated developmental stages, each expressed as percentage of total nuclei in the respective zone(s) as determined by DAPI staining. Data are the mean ± SD (E20, $n = 8$; E24, $n = 4$; E28, $n = 4$; E32, $n = 5$; E36, $n = 4$; P1, $n = 8$). Scale bar = 1 mm in B; 100 μm in C; 50 μm in D–I.

of the noncycling cells lacked immunoreactivity for beta-III tubulin, rendering it unlikely that these cells were newborn neurons that had inherited the Pax6 protein (data not shown). As expected, the proportion of cycling cells in the Pax6− & Tbr2− subpopulation was minor, especially in the OSVZ (Fig. 2C), consistent with the vast majority of the cells in this subpopulation being newborn neurons.

Cell cycle parameters of progenitor subpopulations in the germinal zones of P1 ferret neocortex

Length of total cell cycle and S-phase

Starting with P1 ferret kits, we performed cumulative labeling with the thymidine analogue EdU for up to 48 hours to determine the cell cycle parameters of the various Pax6±, Tbr2± progenitor subpopulations in the three neocortical germinal zones (Fig. 3A,B). We first determined the duration of their total cell cycle minus S-phase (T_C–T_S) and the duration of S-phase (T_S) (Fig. 3C, Table 1), taking into account the fact that only between 60% and 100% of the cells in a given subpopulation and germinal zone were cycling (Figs. 2C, 3C, arrows), data that were corroborated by determining the so-called growth fraction of the respective progenitor subpopulation from the plateau of the EdU labeling index (Fig. 3C, dashed horizontal lines). The total cell cycle length ranged from 37.9 hours in Pax6− & Tbr2+ progenitors in the ISVZ (likely bIPs) to 68.7 hours in Pax6+ & Tbr2− progenitors in the OSVZ
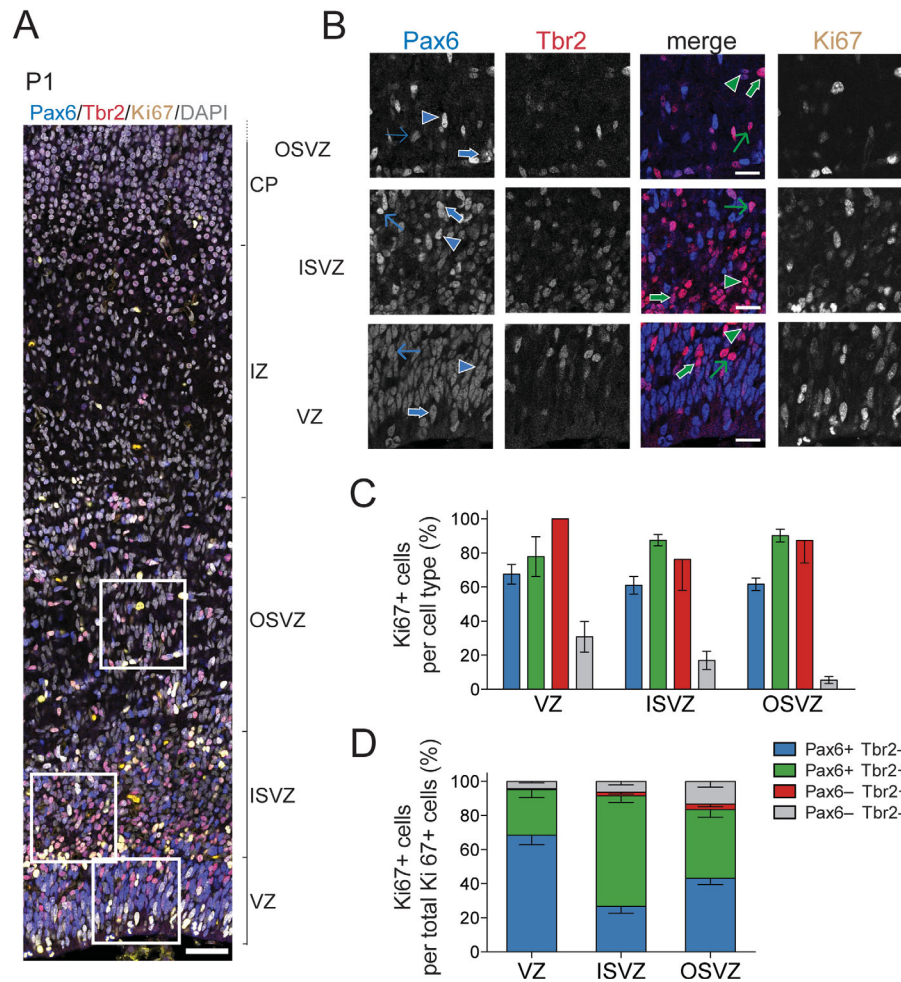
Figure 2. Proportion of cycling progenitors among the various cell subpopulations in the germinal zones of P1 ferret neocortex. **A:** Triple immunofluorescence for Pax6 (blue), Tbr2 (red), and Ki67 (yellow), combined with DAPI staining (gray), on a 20-μm coronal cryosection of P1 ferret neocortex (1-μm optical section). Scale bar, 50 μm. **B:** Higher magnification of the areas indicated in A, showing immunofluorescence for Pax6 (first column, blue in merged images), Tbr2 (second column, red in merged images), Pax6 & Tbr2 (merge, third column), and Ki67 (fourth column). Selected cells are indicated as follows: blue arrowheads, Pax6+ Tbr2− Ki67−; thin blue arrows, Pax6+ Tbr2− Ki67+ (low Ki67 intensity); thick blue arrows, Pax6+ Tbr2− Ki67+ (high Ki67 intensity); green arrowheads, Pax6+ Tbr2+ Ki67−; thin green arrows, Pax6+ Tbr2+ Ki67+ (low Ki67 intensity); thick green arrows, Pax6+ Tbr2+ Ki67+ (high Ki67 intensity). **C:** Quantification of the percentage of Ki67+ cells within each Pax6± & Tbr2± cell subpopulation (see key) for each of the three germinal zones of P1 ferret neocortex. Data are the mean ± SD (n = 8). **D:** Quantification of the percentage of the Ki67+ cells of each Pax6± & Tbr2± cell subpopulation (see key) within the total Ki67+ cells for each of the three germinal zones of the P1 ferret neocortex. Data are the mean ± SD (n = 8). Scale bar = 50 μm in A; 20 μm in B.

(likely bRG) (Table 1). The duration of S-phase in the different progenitor subpopulations showed a much greater variation, ranging from 1.9 hours (bIPs in ISVZ) to 22.6 hours (bRG in OSVZ) (Table 1). These results place the cell cycle duration of ferret neocortical progenitors closer to those of primates (Betizeau et al., 2013; Kornack and Rakic, 1998; Lukaszewicz et al., 2005) than to rodents (Arai et al., 2011; Takahashi et al., 1995), consistent with the overall longer neurogenic period in the gyrencephalic species studied so far.

Length of G2-phase

Next, we determined the duration of G2 in the major progenitor subpopulations by measuring the kinetics of EdU incorporation into either Pax6+ or Tbr2+ cells in mitosis (PH3+) (Fig. 4A–F). (Because of the limited number of fluorescence channels, we could only perform either Pax6 or Tbr2 single immunofluorescence, but not Pax6 and Tbr2 double immunofluorescence, together with PH3 and EdU detection.) The time of half-maximal EdU incorporation, indicative of the avarage duration of G2 (T_{G2}), was similar for the progenitor
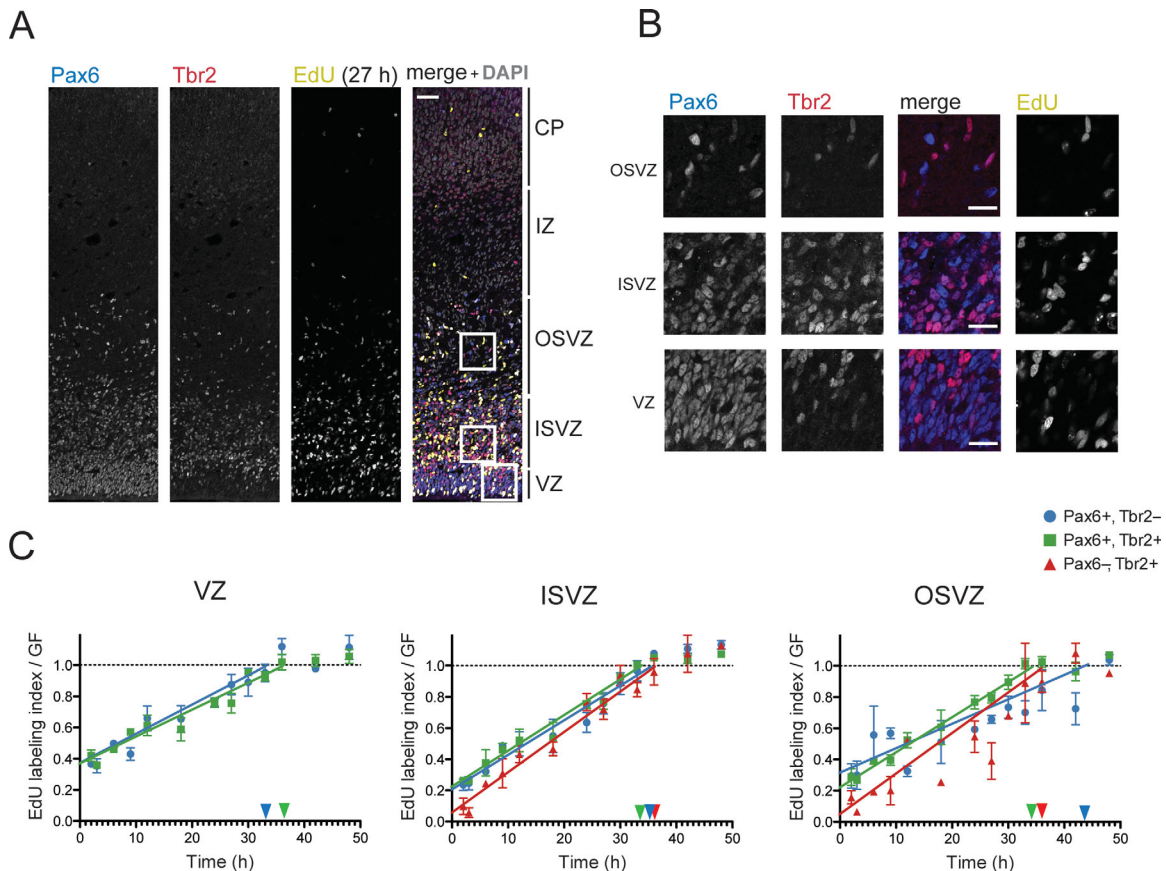
Figure 3. Cumulative EdU labeling of P1 ferret neocortical progenitors. **A:** Triple (immuno)fluorescence for Pax6 (blue in merged image), Tbr2 (red in merged image), and EdU (yellow in merged image), combined with DAPI staining (gray in merged image), on a 20-μm coronal cryosection of P1 ferret neocortex (1-μm optical section), after 27 hours of cumulative EdU labeling. **B:** Higher magnification of the areas indicated in A, showing immunofluorescence for Pax6 (first column, blue in merged images), Tbr2 (second column, red in merged images), Pax6 & Tbr2 (merge, third column), and EdU (fourth column). **C:** Cumulative EdU labeling of Pax6+ & Tbr2− (blue circles), Pax6+ & Tbr2+ (green squares), and Pax6− & Tbr2+ (red triangles) progenitors in each of the three germinal zone of P1 (start of EdU labeling) ferret neocortex. Color-coded horizontal dashed lines indicate the growth fraction of the respective progenitor subpopulation as determined from the plateau of cumulative labeling. Color-coded arrows on the Y-axes indicate the proportion of cycling progenitors in the respective cell subpopulation as determined in Figure 2C. Color-coded arrowheads on the X-axes indicate the time at which the respective progenitor subpopulation is predicted to reach the plateau (corresponding to T_C-T_S). Data are the mean $\pm$ SEM ($n = 3$ for all time points, except for 2, 6, 9, and 18 hours, for which $n = 2$; in the latter cases, error bars indicate the variation of the individual values from the mean). Scale bar = 50 μm in A; 20 μm in B.

subpopulations analyzed, ranging from 1.7 to 2.2 hours (Table 1).

In a separate set of experiments, the proportions of mitotic Pax6+ & Tbr2−, Pax6+ & Tbr2+, Pax6− & Tbr2+, and Pax6− & Tbr2− progenitors were found to be similar (Fig. 4G) to those of the respective entire cycling cell subpopulations (Fig. 2D). These data imply that the T_{G2} values for the Pax6+ progenitor subpopulations reflected largely the joint contribution of the Pax6+ & Tbr2− and Pax6+ & Tbr2+ progenitor subpopulations in the respective germinal zones, and the T_{G2} values for the Tbr2+ progenitor subpopulations largely the contribution of the Pax6+ & Tbr2+ progenitor subpopulations.

Length of M-phase

We determined the duration of mitosis (T_M) from the proportion of mitotic cells within each cycling progenitor subpopulation and the duration of the total cell cycle of that subpopulation. T_M values ranged from 0.5 to 2.0 hours (Table 1).

Length of G1-phase

We used the T_C, T_S, averaged T_{G2}, and T_M values to calculate the duration of G1 (T_{G1}) for each progenitor subpopulation (Table 1). The duration of G1 in the various progenitor subpopulations was remarkably similar, with an average T_{G1} value of 32.3 hours, with the exception
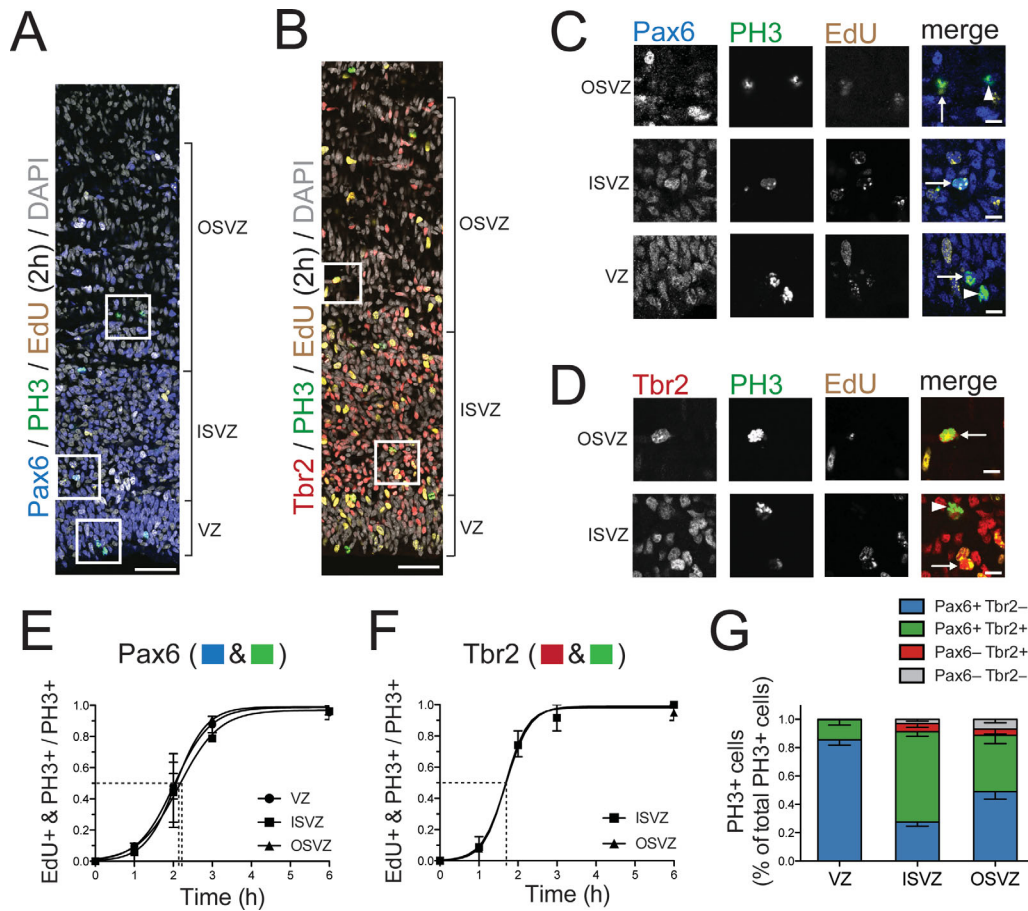
Figure 4. Cumulative EdU labeling of mitotic P1 ferret neocortical progenitors. **A,C:** Triple (immuno)fluorescence for either Pax6 (**A,** blue) or Tbr2 (**C,** red), phosphohistone H3 (PH3, green), and EdU (yellow), combined with DAPI staining (gray), on a 10-μm coronal cryosection of P1 ferret neocortex after 2 hours of EdU labeling (single 1-μm optical section). **B,D:** Higher magnification of the regions indicated in A and C, respectively. **B:** Arrows indicate Pax6+ PH3+ EdU+ mitotic cells and arrowheads Pax6+ PH3+ EdU− mitotic cells. **D:** Arrows indicate Tbr2+ PH3+ EdU+ mitotic cells and the arrowhead a Tbr2+ PH3+ EdU− mitotic cell. **E,F:** Cumulative EdU labeling of mitotic Pax6+ cells (**E**) and mitotic Tbr2+ cells (**F**) in the indicated germinal zones of P1 ferret neocortex. Fitted sigmoidal curves are shown. Dashed lines indicate the half-maximal labeling time, corresponding to the average duration of G2 (2.0, 2.2, and 2.1 hours for Pax6+ progenitors in VZ, ISVZ, and OSVZ, respectively, and 1.7 hours for Tbr2+ progenitors in ISVZ and OSVZ). **G:** Quantification of the proportion of the PH3+ cells of each Pax6± & Tbr2± cell subpopulation (see key) within the total PH3+ cells for each of the three germinal zones of the P1 ferret neocortex. Data are mean ± SEM ($n = 9$). Scale bar = 50 μm in A; 20 μm in B–D.

of the Pax6+ & Tbr2− progenitors in the OSVZ (i.e., bRG) which displayed a substantially longer G1 phase of 42.5 hours (Table 1).

S-phase is the most variable cell cycle phase in the progenitor subpopulations of P1 ferret neocortex

Thus, having determined the duration of G1-, S-, G2-, and M-phases of the Pax6+ & Tbr2−, Pax6+ & Tbr2+, and Pax6− & Tbr2+ progenitor subpopulations in the P1 ferret VZ, ISVZ, and OSVZ, it emerges that by far the greatest variation occurs in the duration of S-phase (Fig. 5A). We sought to corroborate this by an independent method and therefore examined the pattern of

PCNA staining in each progenitor subpopulation. Cortical progenitor cells in S-phase typically exhibit a punctate PCNA staining pattern (Arai et al., 2011; Betizeau et al., 2013). We performed immunofluorescence for PCNA in combination with Pax6 and Tbr2 immunostaining in the developing ferret neocortex from E20 to P1 (Fig. 6A–C). This revealed the presence of punctate PCNA staining in all three germinal zones (Fig. 6C) among the Pax6+ & Tbr2−, Pax6+ & Tbr2+, and Pax6− & Tbr2+ progenitor subpopulations at all stages analyzed, although at varying proportions (Fig. 6D). The percentages of cells in S-phase, as determined from the proportion of PCNA+ nuclei showing a punctate staining pattern, for the three progenitor subpopulations in the three germinal zones at P1 (Fig. 6D, column

bars) were comparable to those calculated from the cumulative EdU labeling data (Figs. 6D, arrows, 5B, Table 1).

Depicting the duration of each cell cycle phase as a proportion of the total cell cycle (Fig. 5B, Table 1) rather than as absolute time (Fig. 5A) revealed three distinct cell cycle parameter profiles. The first one is shared by APs, Pax6+ & Tbr2+ progenitors in the VZ, and bRG in the OSVZ, which spend approximately one-third of their cell cycle in S-phase (32.4%, 35.1%, and 32.9%, respectively) and close to 60% in G1 (61.2%, 61.0%, and 61.8%, respectively). The second one is characteristic of Pax6+ & Tbr2+ progenitors in both the ISVZ and OSVZ and of bRG in the ISVZ, which spend around 20% of the cell cycle in S-phase (21.5%, 23.0%, and 19.5%, respectively) and slightly over 70% in G1 (72.8%, 72.1%, and 73.7%, respectively). The third one is seen in bIPs in both the ISVZ and OSVZ, which spend around 85% of their cell cycle in G1 (85.2% and 85.3%, respectively) and less than 10% in S-phase (5.0% and 8.0%, respectively) (Fig. 5B, Table 1).

DISCUSSION

Progenitor types in ferret corticogenesis

We first investigated the proportions of neural progenitors along cortical neurogenesis in the ferret. Our results are consistent with previous studies (Martinez-Cerdeno et al., 2012; Poluch and Juliano, 2015), complementing them by analyzing neural progenitor populations throughout all cell cycle phases and proliferative areas, both before the onset of neurogenesis (E20, E24) and along the subsequent stages of this process (E28, E32, E36, P1). The proportions of Pax6+ & Tbr2− cells (APs in the VZ, and bRG in the SVZ) that we observed were similar to those reported before (Fietz et al., 2010; Reillo and Borrell, 2012; Reillo et al., 2011); it can be speculated that certain subpopulations of APs and bRG are in a state of quiescence, poised for proliferation during the forthcoming gliogenic period. We observed a significant drop in the proportion of neurogenic bIPs in the SVZ, occurring after the onset of neurogenesis and concomitant with the expansion of the SVZ associated with the appearance of the OSVZ (Fig. 1L). These progenitors have been considered fundamental for the generation of neocortical neurons and for cortical surface expansion (Kriegstein et al., 2006). However, they do not seem to play a major role in ferret corticogenesis, where they are far less abundant than in mouse (Arai et al., 2011) or primate — both macaque (Betizeau et al., 2013) and human (Hansen et al., 2010) — cortices, throughout the neurogenic period and across different areas, although a greater
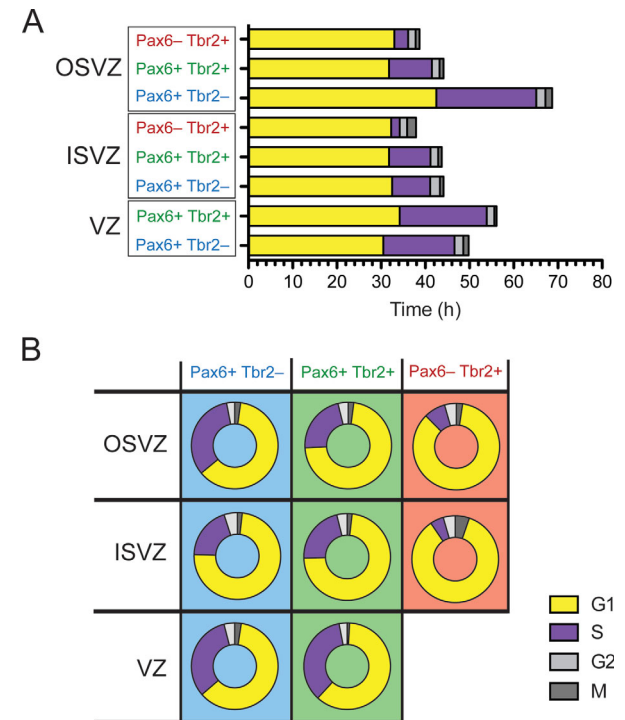

Figure 5. Cell cycle parameters of P1 ferret neocortical progenitors. **A:** Average duration of cell cycle phases (G1, yellow; S, purple; G2, white; M, gray) for the indicated progenitor type and germinal zone. **B:** Proportional contribution of cell cycle phases to total cell cycle for the indicated progenitor type and germinal zone.

proportion of these progenitors is actively cycling in the ferret (Poluch and Juliano, 2015; Reillo and Borrell, 2012; Reillo et al., 2011; present study).

Pax6+ & Tbr2+ in the SVZ are proliferative BPs

The most abundant progenitor population in the ferret SVZ is that of Pax6+ & Tbr2+ cells. Given their transcription factor expression, halfway between that of self-renewing bRG (Fietz et al., 2010; Gertz et al., 2014) and that of bIPs (Englund et al., 2005), and considering their cell cycle profile (Fig. 5E), which is consistent with these cells being both self-renewing and neurogenic, we propose that these progenitors are a proliferative type of BPs and also able to undergo neurogenic divisions. Although a proportion of the different types of bRG in the macaque are positive for Tbr2 as well as Pax6 (Betizeau et al., 2013), no basal process-bearing progenitors in the ferret neocortex are Tbr2+ (Fietz et al., 2010). One may speculate that the bRG population in this species could be less diverse than in primates. Indeed, the proportion of bRG bearing two processes (bp-RG/bRG-both-P) is much lower in the
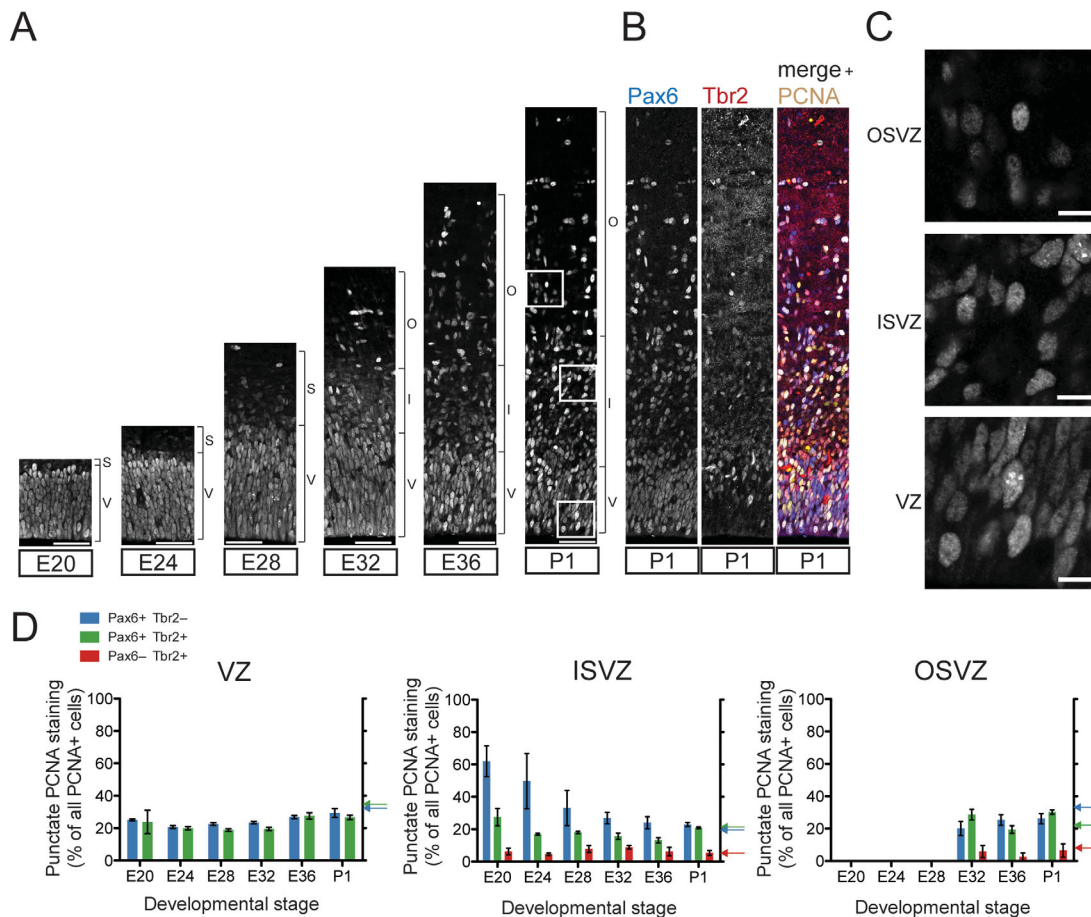
Figure 6. PCNA staining of developing ferret neocortex to determine the proportion of progenitors in S-phase. **A:** Immunofluorescence for PCNA on 20-µm coronal cryosections of ferret neocortex at the indicated stages (single 1-µm optical sections). V, ventricular zone; S, sub-ventricular zone; I, inner subventricular zone; O, outer subventricular zone. **B:** Right: same PCNA immunofluorescence (yellow) of P1 ferret neocortex as in A, combined with Pax6 (left, blue in merged image on right) and Tbr2 (middle, red in merged image on right) immunofluo-rescence. **C:** Higher magnification of the PCNA-stained regions indicated in A. **D:** Quantification of the percentage of PCNA nuclei showing punctate staining, indicative of S-phase, within each Pax6± & Tbr2± progenitor subpopulation (see key) for each of the three germinal zones of ferret neocortex at the indicated developmental stages. Data are mean ± SEM (n = 5 for E20, E32, P1; n = 4 for E24, E28, E36). Color-coded arrows on the right Y-axes indicate the percentages of progenitors in S-phase at P1, as calculated from the cumulative EdU labeling data (Fig. 3C, Table 1). Scale bar = 50 µm in A; 10 µm in C.

OSVZ of the developing ferret neocortex (10–15% of OSVZ mitoses at P2; Pilz et al., 2013) than in the maca-que (50% of OSVZ mitoses at E78; Betizeau et al., 2013). It is also possible that part of these cells could correspond to the tbRG population identified by live imaging in the macaque OSVZ, which are present in a proportion similar to that of Pax6+ & Tbr2+ cells in this area (Betizeau et al., 2013).

Pax6+ & Tbr2+ progenitors in the VZ

Pax6+ & Tbr2+ progenitors are also present in the VZ. In the mouse, these cells have been considered to be newborn bIPs (Arai et al., 2011), although part of them could also correspond to apical intermediate pro-genitors (previously called short neural precursors) (Stancik et al., 2010). In the case of the P1 ferret VZ, a

fraction of the ventricular mitoses (14.1%) is Pax6+ & Tbr2+, whereas roughly twice as many (26.9%) of the cycling progenitors are positive for both markers. Tak-ing into consideration their cell cycle profile, resembling that of APs and hence potentially reflecting a high self-renewing potential (Fig. 5B), and the basal location of the majority of these cells within the VZ, this is consist-ent with a scenario in which some APs would turn on Tbr2 expression before undergoing an asymmetric divi-sion to generate a new Pax6+ & Tbr2+ AP and a new-born proliferative bIP that would then migrate basally into the SVZ, completing its cell cycle there.

Diversity of progenitors and gyrencephaly

We hypothesize, based on previous work and the evi-dence presented here, that the diversity of SVZ

progenitor types is correlated with the degree of cortical surface folding. Highly gyrencephalic primate brains appear to have a greater variety of bRG types, and some also a higher proportion of neurogenic bIPs (Betizeau et al., 2013; Hansen et al., 2010), compared with the less gyrated ferret brain (Gertz et al., 2014; Reillo and Borrell, 2012; Reillo et al., 2011; present study), which in turn presents a greater proportion of bRG and proliferative bIPs than the lissencephalic mouse (Arai et al., 2011; Shitamukai et al., 2011; Wang et al., 2011). Interestingly, the marmoset, a near-lissencephalic primate, displays a lower proportion of Tbr2+ mitoses than the ferret (Kelava et al., 2012). In addition, a chemically induced ferret lissencephaly model displays an overall loss of Tbr2-positive dividing cells throughout the cortical wall at P0, accompanied by a loss of radial glial fibers, implying a loss of bIPs and bRG (Poluch and Juliano, 2015). Taken together, these studies can be interpreted as further support for the hypothesis that the abundance of certain progenitor types, especially proliferative BPs, is essential for the appearance of gyrencephaly.

Cell cycle length of ferret neocortical progenitors

Our cell cycle analyses complement a pioneering study that analyzed T_C and T_S in the different proliferative areas of the ferret neocortex at P0 and P6 (Reillo and Borrell, 2012). If we analyze our data in an analogous way, considering the entire cycling population in each proliferative area, we obtain values with similar trends: longer total cell cycle in VZ and OSVZ, and longer S-phase in the VZ than in either SVZ area (VZ: T_C = 49.4 hours, T_S = 13.3 hours; ISVZ: T_C = 43.0 hours; T_S = 7.0 hours; OSVZ: T_C = 48.7 hours; T_S = 6.7 hours). However, cycling cells at P1 display different values, with an overall longer T_C and shorter T_S than at P0 (Reillo and Borrell, 2012); this could reflect either methodological differences (because our study used a greater number of biological replicates) or an underlying biological significance, whereby great changes in the dynamics of the cell cycle of neural progenitors would occur in the first postnatal days, perhaps as a consequence of the change of environment elicited by birth.

S-phase is the main source of cell cycle variation

Surprisingly, the main source of variation in cell cycle length between the different progenitor types in ferret neocortex was not T_{G1}, as is the case for the two major cortical progenitor classes in the mouse (Arai et al., 2011), but T_S (Fig. 5A, Table 1). Specifically, the absolute length of S-phase varied as much as 10-fold, whereas that of G1 varied by less than 1.5-fold (Fig. 5A). Thus, our data extend the so-called cell cycle length hypothesis, which postulates, based on observations in the mouse, that G1-phase is a time window for cell fate determinants to act upon neocortical progenitors (Borrell and Calegari, 2014; Calegari and Huttner, 2003; Götz and Huttner, 2005; Salomoni and Calegari, 2010). However, when the relative proportion of the total cell cycle duration spent in each phase is considered, our results follow the established paradigm in that more differentiated cells, such as bIPs, spend a greater portion of their cell cycle in G1 compared with progenitors with greater self-renewal capacity (Fig. 5B).

A recent study in the macaque determined the total cell cycle duration of cortical progenitors by time-lapse imaging on organotypic slices and the relative proportions of G1- and S-phase by immunohistochemical analyses (Betizeau et al., 2013). This study reported changes in the proportions of G1- and S-phase in the VZ and OSVZ between E65 and E78, with the cell cycle profiles being somewhat similar to those of the ferret. Of note, the average cell cycle length of progenitors undergoing proliferative divisions was found to be shorter than that of progenitors undergoing differentiative ones (Betizeau et al., 2013). It therefore appears that, depending on the species and progenitor type, the repertoire of changing cell cycle phases in terms of absolute duration versus relative proportion is greater than previously assumed.

On a more general note, our work suggests, therefore, that there is not a conserved developmental program in mammals for increasing neuron output or heterogeneity. This could be due either to intrinsic differences among the mouse, primate, and ferret neocortices, such as differences in progenitor diversity as outlined above, or, alternatively, to possible alterations in cell cycle dynamics brought about by tissue culture conditions (Breunig et al., 2011).

A shortening of S-phase in differentiating neocortical progenitors has been described in the mouse, and is likely to be a consequence of a decrease in the quality control of DNA replication of cells committed to neurogenic divisions (Arai et al., 2011). This could in turn be related to the genomic heterogeneity of the mature brain, thought to be a source of neural diversity (Bushman and Chun, 2013). In the ferret, the extent of S-phase shortening is greater than in the mouse (Arai et al., 2011); this could be a consequence of the greater progenitor number and neuron output of a gyrencephalic brain, especially during the generation of supragranular layers, compared with a lissencephalic one.

Our work suggests the existence of different evolutionary strategies leading to increases in neuron output and neocortical expansion. These mechanisms would operate both at the level of progenitor abundance and at that of cell cycle dynamics in each progenitor type. The moderately gyrencephalic ferret brain will undoubtedly remain a very useful model in the field of neocortical development, allowing comparisons between species with different degrees of cortical folding.

CONFLICT OF INTEREST STATEMENT

The authors declare no conflicts of interest.

ROLE OF AUTHORS

All authors had full access to all the data in the study and take responsibility for the integrity of the data and the accuracy of the data analysis. Study concept and design: MTG, YA, WBH. Acquisition of data: MTG, YJC. Analysis and interpretation of data: MTG, WBH. Writing of the manuscript: MTG, WBH.

LITERATURE CITED

Arai Y, Pulvers JN, Haffner C, Schilling B, Nusslein I, Calegari F, Huttner WB. 2011. Neural stem and progenitor cells shorten S-phase on commitment to neuron production. Nat Commun 2:154.

Betizeau M, Cortay V, Patti D, Pfister S, Gautier E, Bellemin-Ménard A, Afanassieff M, Huissoud C, Douglas RJ, Kennedy H, Dehay C. 2013. Precursor diversity and complexity of lineage relationships in the outer subventricular zone of the primate. Neuron 80:442–457.

Borrell V, Calegari F. 2014. Mechanisms of brain evolution: regulation of neural progenitor cell diversity and cell cycle length. Neurosci Res 86:14–24.

Borrell V, Reillo I. 2012. Emerging roles of neural stem cells in cerebral cortex development and evolution. Dev Neurobiol 72:955–971.

Breunig JJ, Haydar TF, Rakic P. 2011. Neural stem cells: historical perspective and future prospects. Neuron 70:614–625.

Bushman DM, Chun J. 2013. The genomically mosaic brain: aneuploidy and more in neural diversity and disease Semin Cell Dev Biol 24:357–369.

Calegari F, Huttner WB. 2003. An inhibition of cyclin-dependent kinases that lengthens, but does not arrest, neuroepithelial cell cycle induces premature neurogenesis. J Cell Sci 116:4947–4955

Calegari F, Haubensak W, Haffner C, Huttner WB. 2005. Selective lengthening of the cell cycle in the neurogenic subpopulation of neural progenitor cells during mouse brain development. J Neurosci 25:6533–6538.

Caviness VS Jr, Takahashi T. 1995. Proliferative events in the cerebral ventricular zone. Brain Dev 17:159–163.

Cheung AF, Pollen AA, Tavare A, DeProto J, Molnar Z. 2007. Comparative aspects of cortical neurogenesis in vertebrates. J Anat 211:164–176.

Davis JA, Reed RR. 1996. Role of Olf-1 and Pax-6 transcription factors in neurodevelopment. J Neurosci 16:5082–5094.

Dehay C, Kennedy H. 2007. Cell-cycle control and cortical development. Nat Rev Neurosci 8:438–450.

Englund C, Fink A, Lau C, Pham D, Daza RA, Bulfone A, Kowalczyk T, Hevner RF. 2005. Pax6, Tbr2, and Tbr1 are expressed sequentially by radial glia, intermediate progenitor cells, and postmitotic neurons in developing neocortex. J Neurosci 25:247–251.

Fietz SA, Huttner WB. 2011. Cortical progenitor expansion, self-renewal and neurogenesis—a polarized perspective. Curr Opin Neurobiol 21:23–35.

Fietz SA, Kelava I, Vogt J, Wilsch-Brauninger M, Stenzel D, Fish JL, Corbeil D, Riehn A, Distler W, Nitsch R, Huttner WB. 2010. OSVZ progenitors of human and ferret neocortex are epithelial-like and expand by integrin signaling. Nat Neurosci 13:690–699.

Fish JL, Kennedy H, Dehay C, Huttner WB. 2008. Making bigger brains—the evolution of neural-progenitor-cell division. J Cell Sci 121:2783–2793.

Florio M, Huttner WB. 2014. Neural progenitors, neurogenesis and the evolution of the neocortex. Development 141:2182–2194.

Franco SJ, Muller U. 2013. Shaping our minds: stem and progenitor cell diversity in the mammalian neocortex. Neuron 77:19–34.

Gertz CC, Lui JH, Lamonica BE, Wang X, Kriegstein AR. 2014. Diverse behaviors of outer radial glia in developing ferret and human cortex. J Neurosci 34:2559–2570.

Götz M, Huttner WB. 2005. The cell biology of neurogenesis. Nat Rev Mol Cell Biol 6:777–788.

Hansen DV, Lui JH, Parker PR, Kriegstein AR. 2010. Neurogenic radial glia in the outer subventricular zone of human neocortex. Nature 464:554–561.

Haubensak W, Attardo A, Denk W, Huttner WB. 2004. Neurons arise in the basal neuroepithelium of the early mammalian telencephalon: a major site of neurogenesis. Proc Natl Acad Sci U S A 101:3196–3201.

Kelava I, Reillo I, Murayama AY, Kalinka AT, Stenzel D, Tomancak P, Matsuzaki F, Lebrand C, Sasaki E, Schwamborn JC, Okano H, Huttner WB, Borrell V. 2012. Abundant occurrence of basal radial glia in the subventricular zone of embryonic neocortex of a lissencephalic primate, the common marmoset *Callithrix jacchus*. Cereb Cortex 22:469–481.

Key G, Petersen JL, Becker MH, Duchrow M, Schlüter C, Askaa J, Gerdes J. 1993. New antiserum against Ki-67 antigen suitable for double immunostaining of paraffin wax sections. J Clin Pathol 46:1080–1084.

Kornack DR, Rakic P. 1998. Changes in cell-cycle kinetics during the development and evolution of primate neocortex. Proc Natl Acad Sci U S A 95:1242–1246.

Kriegstein A, Alvarez-Buylla A. 2009. The glial nature of embryonic and adult neural stem cells. Annu Rev Neurosci 32:149–184.

Kriegstein A, Noctor S, Martinez-Cerdeno V. 2006. Patterns of neural stem and progenitor cell division may underlie

evolutionary cortical expansion. Nat Rev Neurosci 7: 883–890.

LaMonica BE, Lui JH, Hansen DV, Kriegstein AR. 2013. Mitotic spindle orientation predicts outer radial glial cell generation in human neocortex. Nat Commun 4:1665.

Lange C, Huttner WB, Calegari F. 2009. Cdk4/cyclinD1 over-expression in neural stem cells shortens G1, delays neurogenesis, and promotes the generation and expansion of basal progenitors. Cell Stem Cell 5:320–331.

Lewitus E, Kelava I, Huttner WB. 2013. Conical expansion of the outer subventricular zone and the role of neocortical folding in evolution and development. Front Hum Neurosci 7:424.

Lui JH, Hansen DV, Kriegstein AR. 2011. Development and evolution of the human neocortex. Cell 146:18–36.

Lukaszewicz A, Savatier P, Cortay V, Giroud P, Huissoud C, Berland M, Kennedy H, Dehay C. 2005. G1 phase regulation, area-specific cell cycle control, and cytoarchitectonics in the primate cortex. Neuron 47:353–364.

Martinez-Cerdeno V, Cunningham CL, Camacho J, Antczak JL, Prakash AN, Cziep ME, Walker AI, Noctor SC. 2012. Comparative analysis of the subventricular zone in rat, ferret and macaque: evidence for an outer subventricular zone in rodents. PLoS One 7:e30178.

Miyata T, Kawaguchi A, Saito K, Kawano M, Muto T, Ogawa M. 2004. Asymmetric production of surface-dividing and non-surface-dividing cortical progenitor cells. Development 131:3133–3145.

Noctor SC, Scholnicoff NJ, Juliano SL. 1997. Histogenesis of ferret somatosensory cortex. J Comp Neurol 387:179–193.

Noctor SC, Martinez-Cerdeno V, Ivic L, Kriegstein AR. 2004. Cortical neurons arise in symmetric and asymmetric division zones and migrate through specific phases. Nat Neurosci 7:136–144.

Nowakowski RS, Lewin SB, Miller MW. 1989. Bromodeoxyuridine immunohistochemical determination of the lengths of the cell cycle and the DNA-synthetic phase for an anatomically defined population. J Neurocytol 18:311–318.

Pilaz LJ, Patti D, Marcy G, Ollier E, Pfister S, Douglas RJ, Betizeau M, Gautier E, Cortay V, Doerflinger N, Kennedy H, Dehay C. 2009. Forced G1-phase reduction alters mode of division, neuron number, and laminar phenotype in the cerebral cortex. Proc Natl Acad Sci U S A 106: 21924–21929.

Pilz GA, Shitamukai A, Reillo I, Pacary E, Schwausch J, Stahl R, Ninkovic J, Snippert HJ, Clevers H, Godinho L, Guillemot F, Borrell V, Matsuzaki F, Gotz M. 2013. Amplification of progenitors in the mammalian telencephalon includes a new radial glial cell type. Nat Commun 4: 2125.

Poluch S, Juliano SL. 2015. Fine-tuning of neurogenesis is essential for the evolutionary expansion of the cerebral cortex. Cereb Cortex 25:346–364.

Reillo I, Borrell V. 2012. Germinal zones in the developing cerebral cortex of ferret: ontogeny, cell cycle kinetics, and diversity of progenitors. Cereb Cortex 22:2039–2054.

Reillo I, de Juan Romero C, Garcia-Cabezas MA, Borrell V. 2011. A role for intermediate radial glia in the tangential expansion of the mammalian cerebral cortex. Cereb Cortex 21:1674–1694.

Salomoni P, Calegari F. 2010. Cell cycle control of mammalian neural stem cells: putting a speed limit on G1. Trends Cell Biol 20:233–243.

Shitamukai A, Konno D, Matsuzaki F. 2011. Oblique radial glial divisions in the developing mouse neocortex induce self-renewing progenitors outside the germinal zone that resemble primate outer subventricular zone progenitors. J Neurosci 31:3683–3695.

Smart IH, Dehay C, Giroud P, Berland M, Kennedy H. 2002. Unique morphological features of the proliferative zones and postmitotic compartments of the neural epithelium giving rise to striate and extrastriate cortex in the monkey. Cereb Cortex 12:37–53.

Stancik EK, Navarro-Quiroga I, Sellke R, Haydar TF. 2010. Heterogeneity in ventricular zone neural precursors contributes to neuronal fate diversity in the postnatal neocortex. J Neurosci 30:7028–7036.

Takahashi T, Nowakowski RS, Caviness VS, Jr. 1995. The cell cycle of the pseudostratified ventricular epithelium of the embryonic murine cerebral wall. J Neurosci 15:6046–6057.

Taverna E, Götz M, Huttner WB. 2014. The cell biology of neurogenesis: toward an understanding of the development and evolution of the neocortex. Annu Rev Cell Dev Biol 30:465–502.

Wang X, Tsai JW, Lamonica B, Kriegstein AR. 2011. A new subtype of progenitor cell in the mouse embryonic neocortex. Nat Neurosci 14:555–561.

Zilles K, Palomero-Gallagher N, Amunts K. 2013. Development of cortical folding during evolution and ontogeny. Trends Neurosci 36:275–284.